

**Figure 4.** Typical examples of Raman phonon spectra of pentacene taken with different microscope objectives, as labeled. The penetration depth increases from the bottom to the top spectrum of the figure. For better reference, full and dashed lines mark C and H lattice phonons, respectively.

prevailing phase. All these samples were used for the experiments by selecting individual microcrystals with an optical microscope interfaced to a Raman spectrometer (Jobin Yvon T64000 triple monochromator) spanning the lattice-phonon region 10–200  $\text{cm}^{-1}$ . The excitation wavelength was provided by a krypton laser at 752.5 nm to avoid pentacene fluorescence (either exciton-like or from impurities). The incoming power was kept low to avoid crystal damage: the actual power focused on the sample was about 1 mW. The spectra were recorded with the crystal placed on the microscope stage (Olympus BX40), interfaced to the spectrometer, with 10 $\times$ , 50 $\times$ , or 100 $\times$  objectives, reaching a maximum spatial resolution of about 0.9  $\mu\text{m}$ . Raman mapping was automatically achieved after selecting the crystal area to be sampled and the number of points to be checked. The point density was chosen for each experiment according to the size of the crystal and the microscope objective used.

Received: June 30, 2005

Final version: August 23, 2005

Published online: September 15, 2005

- [1] C. D. Dimitrakopoulos, P. R. L. Malenfant, *Adv. Mater.* **2002**, *14*, 99.
- [2] a) M. Bendikov, F. Wudl, D. F. Perepichka, *Chem. Rev.* **2004**, *104*, 4891. b) L.-L. Chua, J. Zaumseil, J.-F. Chang, E. C.-W. Ou, P. K.-H. Ho, H. Sirringhaus, R. H. Friend, *Nature* **2005**, *434*, 194.
- [3] R. Ruiz, D. Choudhary, B. Nickel, T. Toccoli, K.-C. Chang, A. C. Mayer, P. Clancy, J. M. Blakely, R. L. Headrick, S. Iannotta, G. G. Malliaras, *Chem. Mater.* **2004**, *16*, 4497.
- [4] O. D. Jurchescu, J. Baas, T. T. M. Palstra, *Appl. Phys. Lett.* **2004**, *84*, 3061.
- [5] M. Masino, A. Girlando, R. G. Della Valle, E. Venuti, L. Farina, A. Brillante, *Mater. Res. Soc. Symp. Proc.* **2002**, *725*, 149.
- [6] a) C. C. Mattheus, G. A. de Wijs, R. A. de Groot, T. T. M. Palstra, *J. Am. Chem. Soc.* **2003**, *125*, 6323. b) C. C. Mattheus, A. B. Dros, J. Baas, A. Meetsma, J. L. de Boer, T. T. M. Palstra, *Acta Cryst. C* **2001**, *57*, 939. c) C. C. Mattheus, A. B. Dros, J. Baas, G. T. Oostergetel, A. Meetsma, J. L. de Boer, T. T. M. Palstra, *Synth. Met.* **2003**, *138*, 475.
- [7] a) L. F. Drummy, P. K. Miska, D. C. Martin, *J. Mater. Sci.* **2004**, *39*, 4465. b) S. E. Fritz, S. M. Martin, C. D. Frisbie, M. D. Ward, M. F. Toney, *J. Am. Chem. Soc.* **2004**, *126*, 4084.

- [8] F.-J. Meyer zu Heringdorf, M. C. Reuter, R. M. Tromp, *Nature* **2001**, *412*, 517.
- [9] R. B. Campbell, J. M. Robertson, J. Trotter, *Acta Crystallogr.* **1962**, *15*, 289.
- [10] There is no agreement so far on the labeling of pentacene crystal phases, so we retain the labeling we initially adopted, after the names of the crystal structure first authors [5]. The C phase has been also labeled as the 14.5 Å phase (from the d(001) distance [6]), or as the  $\beta$  phase (M. Brinkmann, S. Graff, C. Straupe, J.-C. Wittmann, C. Chaumont, F. Nuesch, A. Aziz, M. Schaer, L. Zuppiroli, *J. Phys. Chem. B* **2003**, *107*, 10531), whereas the H phase has been named as the 14.1 Å phase or the  $\gamma$  phase.
- [11] D. Holmes, S. Kumaraswamy, A. J. Matzger, K. P. Vollhardt, *Chem. Eur. J.* **1999**, *5*, 3399.
- [12] T. Siegrist, Ch. Kloc, J. H. Schön, B. Batlogg, R. C. Haddon, S. Berg, G. A. Thomas, *Angew. Chem. Int. Ed.* **2001**, *40*, 1732.
- [13] E. Venuti, R. G. Della Valle, A. Brillante, M. Masino, A. Girlando, *J. Am. Chem. Soc.* **2002**, *124*, 2128.
- [14] R. G. Della Valle, E. Venuti, A. Brillante, A. Girlando, *J. Chem. Phys.* **2003**, *118*, 807.
- [15] a) A. Brillante, R. G. Della Valle, L. Farina, A. Girlando, M. Masino, E. Venuti, *Chem. Phys. Lett.* **2002**, *357*, 32; b) R. G. Della Valle, E. Venuti, L. Farina, A. Brillante, M. Masino, A. Girlando, *J. Phys. Chem. B* **2004**, *108*, 1822.
- [16] L. Farina, A. Brillante, R. G. Della Valle, E. Venuti, M. Amboage, K. Syassen, *Chem. Phys. Lett.* **2003**, *375*, 490.
- [17] R. W. deBoer, M. E. Gershenson, A. F. Morpurgo, V. Podzorov, *Phys. Status Sol., A* **2004**, *201*, 1302.
- [18] a) R. C. Haddon, X. Chi, M. E. Itkis, J. E. Anthony, D. L. Eaton, T. Siegrist, C. C. Mattheus, T. T. M. Palstra, *J. Phys. Chem. B* **2002**, *106*, 8288. b) M. L. Tiago, J. E. Northrup, S. G. Louie, *Phys. Rev. B* **2003**, *67*, 115212.
- [19] R. G. Della Valle, A. Brillante, L. Farina, E. Venuti, M. Masino, A. Girlando, *Mol. Cryst. Liq. Cryst.* **2004**, *416*, 145.

## One-Dimensional Plasmon Coupling by Facile Self-Assembly of Gold Nanoparticles into Branched Chain Networks\*\*

By Shan Lin, Mei Li, Erik Dujardin,\*  
Christian Girard, and Stephen Mann\*\*

The miniaturization of integrated optical devices is currently limited by challenges associated with the design and implementation of extended planar structures capable of guiding light at the subwavelength scale.<sup>[1–3]</sup> Among several approach-

[\*] Prof. S. Mann, S. Lin, Dr. M. Li  
Centre for Organized Matter Chemistry, School of Chemistry  
University of Bristol, Bristol BS8 1TS (UK)  
E-mail: s.mann@bristol.ac.uk  
Dr. E. Dujardin, Dr. C. Girard  
NanoSciences group, CEMES-CNRS UPR 8011  
29 rue J. Marvig, F-31055 Toulouse Cedex 4 (France)  
E-mail: dujardin@cemes.fr

[\*\*] We thank EPSRC and the European Network of Excellence (NoE) Plasmo-Nano-Devices (Contract No. 507879) for financial support.

es, the controlled organization of metallic nanoparticles into one-dimensional (1D) or two-dimensional (2D) periodic arrays offers a promising strategy to tailor the flux of surface plasmons.<sup>[4–7]</sup> To date, subwavelength optical guiding has only been demonstrated for nanoparticle arrays produced by electron-beam lithography,<sup>[1,5]</sup> which enables precise organization of the metallic dots but is currently limited to a spatial resolution of ca. 50 nm. Nanoparticle-based architectures with increased spatial resolution and complexity should be possible through bottom-up approaches, and in this respect, several recent studies have used templates or interparticle coupling agents to self-assemble preformed metallic nanoparticles, typically 10 nm in diameter. For example, close-packed 2D nanoparticle arrays can be prepared in the presence of templates or coupling agents such as surfactants,<sup>[8]</sup> inorganic crystals,<sup>[9]</sup> or proteins.<sup>[10]</sup> Similarly, 3D architectures based on complementary interparticle interactions involving hydrogen-bonding moieties,<sup>[11]</sup> DNA duplex formation,<sup>[12]</sup> or antigen–antibody<sup>[13]</sup> or streptavidin–biotin<sup>[14]</sup> recognition, have also been reported. Alternatively, the synthesis of anisotropic nanorods can be used to produce uniaxial higher-order structures by spontaneous self-assembly.<sup>[15–19]</sup> Although these approaches show much promise, self- or directed-assembly of nanoparticle assemblies with high component anisotropy (nanowires) and network connectivity remains uncommon at the present time.

The formation of highly anisotropic 1D nanoparticle arrays and their associated collective vectorial properties are of particular interest in nanoelectronics, optoelectronics, nanomagnetism, and biosensor devices.<sup>[20]</sup> Chains of metallic nanoparticles have been prepared by physical confinement in ion-beam-etched tracks in glass<sup>[21]</sup> or porous anodic alumina,<sup>[22]</sup> and by using linear macromolecular or supramolecular templates such as phospholipids,<sup>[23]</sup> polyelectrolytes,<sup>[24–26]</sup> DNA,<sup>[27–33]</sup> peptide nanofibrils,<sup>[34–38]</sup> tubulin,<sup>[39]</sup> bacteriophage and tobacco mosaic virus rods,<sup>[40–42]</sup> and carbon nanotubes.<sup>[43–48]</sup> Alternatively, 1D arrays can be produced, in the absence of templates, by spontaneous self-assembly of isometric nanoparticles with intrinsic magnetic<sup>[49]</sup> or electric dipoles.<sup>[50–52]</sup> In the latter case, linear assembly is induced by partial removal of the organic stabilization shell, which results in an increase in interparticle electric dipole–dipole interactions due to ineffective screening of the semiconductor CdTe crystal dipoles. Chains of metallic nanoparticles have also been reported,<sup>[53–56]</sup> although the origin of the putative dipole interactions and mechanism of chain assembly remain unknown. Unlike semiconductor quantum dots, face-centered cubic (fcc) metallic nanoparticles exhibit no intrinsic electric dipole. However, heterogeneities in surface charge and polarity, associated for example with the non-uniform spatial distribution of capping ligands on different crystal faces,<sup>[56–58]</sup> or nanophase separation in mixed-ligand stabilization layers,<sup>[59]</sup> are possible driving forces for anisotropic self-assembly.

Here we report the preparation of extensive 1D arrays of metallic nanoparticles in water using a facile method based on the controlled ligand exchange of citrate ions adsorbed onto the surface of spherical Au nanoparticles. We show that exchange of

surface adsorbed citrate with the ditopic molecule, mercaptoethyl alcohol (MEA, 2-mercaptoethanol, HS(CH<sub>2</sub>)<sub>2</sub>OH), results in the formation of chain-like superstructures with topological features that are dependent on the extent of surface-ligand substitution. Moreover, rather than depleting the stabilization shell by solvent removal,<sup>[50,54]</sup> we progressively replace the negatively charged citrate ions with covalently bound neutral MEA molecules to produce a mixed-ligand surface layer. In so doing, electrostatic repulsion between the Au nanoparticles is progressively reduced and the stability of the electric dipole associated with charge separation on the nanocrystal surface is potentially enhanced by spatial partitioning of the MEA and citrate capping ligands. As a consequence, highly extended 1D nanoparticle assemblies in the form of discrete chains, bifurcated and looped chains, or interconnected chain networks are assembled spontaneously as the concentration of surface-adsorbed MEA molecules increases. Such complex networks constitute a unique experimental opportunity to test optical waveguiding in subwavelength metallic structures. As a first step in this direction, we show that both chains and networks exhibit strong coupling of surface plasmons in adjacent non-contacting nanoparticles by simulating theoretical far-field extinction spectra that accurately reproduce the experimental absorption spectra.

Addition of an aqueous solution of MEA to a citrate-stabilized Au nanoparticle dispersion at various MEA/Au nanoparticle molar ratios ( $r$ ) typically produced a color change from pale pink to pale blue. Fourier-transform IR (FTIR) spectra showed the absence of a thiol stretching frequency at 2549 cm<sup>-1</sup>, indicating that the added MEA molecules were adsorbed onto the Au nanoparticles. In general, no bulk precipitation was observed except for very high  $r$  values ( $r > 10^9$ ), at which macroscopic aggregates were formed after several days. Figure 1 shows a representative transmission electron microscopy (TEM) image recorded from an air-dried suspension of Au nanoparticles obtained at  $r = 3000:1$  and 24 h after addition of MEA. The sample consisted of looped chains that were

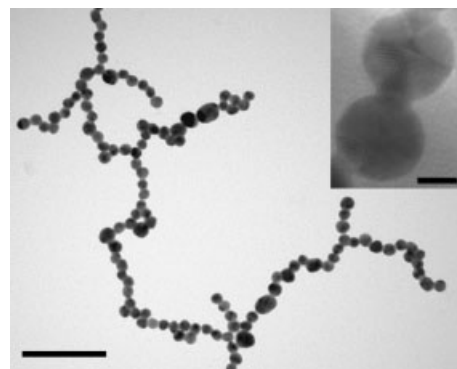


**Figure 1.** TEM image showing region of a self-assembled nanoparticle chain network obtained 24 h after adding MEA to a citrate-stabilized Au sol at  $r = 3000:1$ ; scale bar = 100 nm. Inset: High-magnification TEM image showing organic material at the contact surface between two adjacent nanoparticles in the chain; scale bar = 5 nm.

1–5  $\mu\text{m}$  in length, and consisted of 80–380 isometric 13 nm sized Au nanoparticles. The chains were one nanoparticle wide and comprised bifurcated junctions with outgrowths that were often interconnected to produce an extended branched network. High-resolution TEM images revealed that adjacent nanoparticles were often in close contact within the chains, and covered by a uniform 1 nm thick layer of organic material, which appeared to bridge neighboring Au particles (Fig. 1, inset). Energy dispersive X-ray analysis of the chains yielded gold and sulfur peaks, indicating that MEA molecules were associated with the chain-like arrays. Heating dispersions of the chain networks at 70 °C for 2.5 h did not disrupt the 1D superstructures. In contrast, probe sonication at 4 °C for longer than 5 min resulted in irreversible disassembly.

The influence of MEA concentration on the self-assembly and topology of the Au nanoparticle chains was investigated by optical spectroscopy and TEM using samples prepared at a range of  $r$  values up to approximately  $10^{10}$ :1. For relatively low concentrations of MEA ( $r < 1500$ :1), no change in the 520 nm isotropic surface plasmon band associated with discrete isometric Au nanoparticles was observed after mixing the solutions for 24 h (Fig. 2a, curve i). In marked contrast, a significant reduction in the intensity of the 520 nm band, as well as a new absorption peak at 675 nm, was observed at  $r = 1500$ :1 (Fig. 2a, curve ii). Increasing the MEA concentration to  $r = 3000$ :1 or  $5000$ :1 further reduced the intensity of the 520 nm band, and produced a progressive increase in intensity of the low energy band and spectral red-shift up to a value of 705 nm (Fig. 2a, curve iii). The spectra were relatively unchanged for further increases in  $r$ , although samples prepared in the presence of a large excess of MEA ( $r > 10^9$ :1) showed a single broad band centered at 570 nm, and no restoration of the 520 nm plasmon band (Fig. 2a, curve iv). TEM images corresponding to the above spectral changes showed the presence of isolated nanoparticles or evaporation-induced isotropic aggregates at  $r < 1500$ :1 (Fig. 2b), short chains and discrete nanoparticles at  $1500$ :1 (Fig. 2c), complex chains of increasing length, branching, and interconnectivity between  $3000$  (Fig. 1) and  $10000$ :1 (Fig. 2d), and condensed isotropic aggregates at  $r$  values beyond  $r = 10^6$ :1 (Fig. 2e).

The results imply that spontaneous self-assembly of the Au nanoparticle chain superstructure over a time frame of 24 h is triggered specifically at a MEA threshold level of around  $r = 1500$ :1. The associated uniaxial coupling of the isotropic surface plasmons results in a local field enhancement along the nanoparticle chains, which produces the low-energy longitudinal band observed in the UV-vis spectra. This band progressively increases in intensity and red-shifts towards a value of 705 nm as the extent of chain assembly and network formation become enhanced at higher  $r$  values. However, assembly of the linear superstructures is inhibited in the presence of a vast excess of MEA, with the consequence that large isotropic aggregates are produced in the colloidal sol. Such aggregates are known to exhibit a plasmon resonance in the 540–580 nm range,<sup>[60]</sup> which is higher and lower in wavelength than the isolated nanoparticles or 1D arrays, respectively.

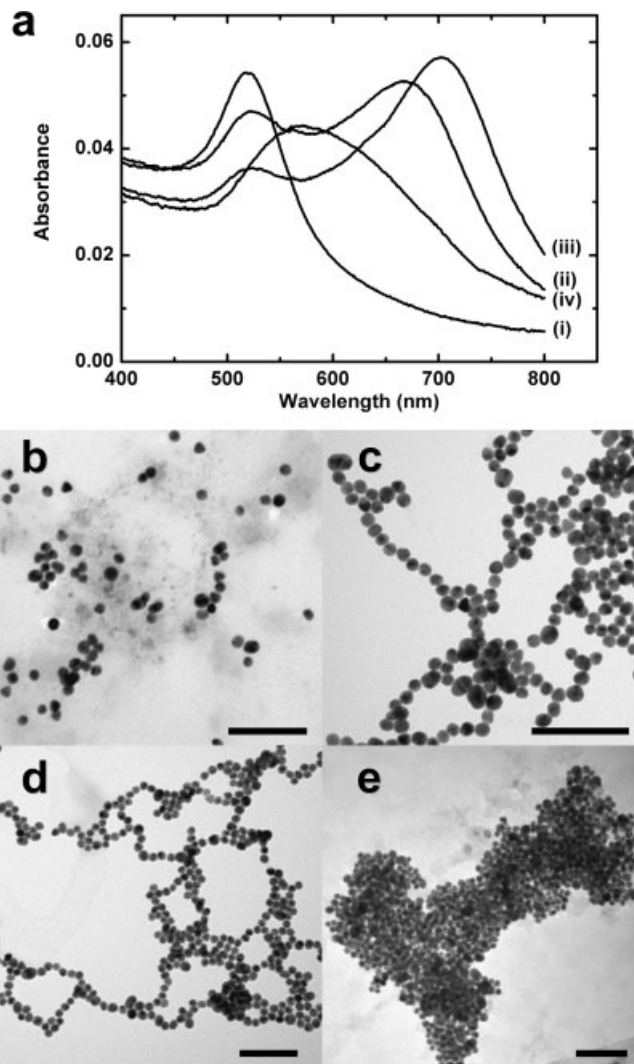


**Figure 2.** a) UV-vis spectra recorded 24 h after addition of MEA to citrate-stabilized Au nanoparticles for  $r$  values of i) 1000:1, ii) 1500:1, iii) 5000:1, and iv)  $10^{10}$ :1. b–e) Corresponding TEM images taken after 24 h at  $r$  values of (b) 1000:1, (c) 1500:1, (d)  $10^4$ :1, and (e)  $10^{10}$ :1. Scale bars are 100 nm.

In order to elucidate the mechanism of chain self-assembly, time-dependent optical spectra were recorded on samples at specific  $r$  values. For example, Figure 3a shows time-lapse UV-vis spectra of solutions prepared at  $r = 5000$ :1. Within 3 h of adding MEA, the 520 nm isotropic plasmon resonance associated with the starting nanoparticle dispersion (Fig. 3a, curve i) was reduced in intensity, and a low-energy shoulder centered at 620 nm appeared (Fig. 3a, curve ii). A continual decrease in the 520 nm band was observed after 7, 24, 48, and 72 h, along with a progressive red-shift in the low-energy shoulder peak to values of 630, 640, 670, and 705 nm, respectively (Fig. 3a, curves iii–vi). No further changes in the 705 nm band were observed. Corresponding TEM images indicated that mainly isolated nanoparticles were initially pres-

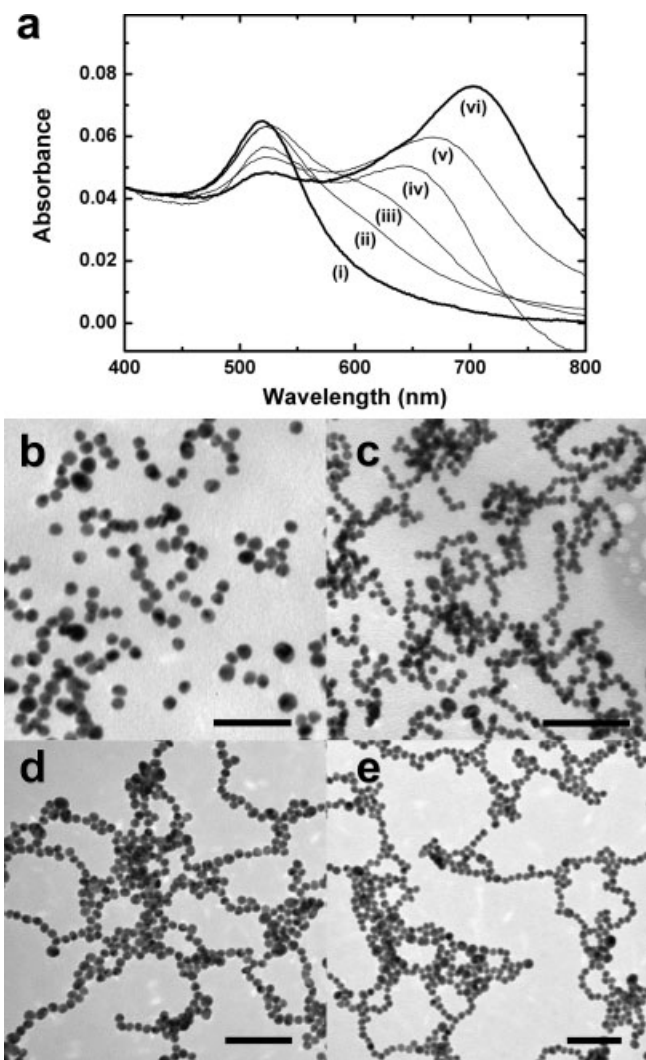


**Figure 3.** a) Time-dependent UV-vis spectra of a Au nanoparticle sol recorded at various times after addition of MEA at  $r=5000:1$ . i) 0 h, ii) 3 h, iii) 7 h, iv) 24 h, v) 48 h, and vi) 72 h. b–e) Corresponding TEM images taken after various times at  $r=5000:1$ : b) 0 h, c) 3 h, d) 24 h, and e) 14 days. Scale bars are 100 nm.

ent after addition of MEA (Fig. 3b), and that self-assembly of short chains generally consisting of less than 20 Au nanoparticles occurred within 3 h (Fig. 3c). With time, the chain-like arrays increased in length and developed increasing numbers of bifurcations and enclosed loops, such that extended networks of interconnected nanoparticle chains were produced within 24 h (Fig. 3d). These superstructures remained unchanged even for prolonged incubation times, such as two weeks (Fig. 3e). The results were consistent with the slow unidirectional self-assembly of Au nanoparticles in close contact, and the progressive formation of a low-energy longitudinal surface plasmon band due to strong uniaxial coupling along the linear array. The wide range of different chain morphologies observed in the extended networks accounts for the broadness of the emerging longitudinal plasmon band and the absence of isobestic points in the time-dependent spectra.

Experimental optical spectra associated with the presence of discrete Au nanoparticles, extended nanoparticle chains, or condensed isotropic aggregates were theoretically simulated (see Experimental). The simulated extinction spectrum of a dispersion of isolated 13 nm diameter Au nanoparticles (Fig. 4a, curve i) showed a single absorption peak at 520 nm, which was in agreement with the experimental results (e.g., Fig. 3a, curve i). Similarly, the calculated spectrum of a densely packed (fcc) isotropic aggregate containing 245 nanoparticles spaced 1 nm apart revealed a large broad absorption centered around 580–600 nm (Fig. 4a, curve ii), consistent with previously reported spectra.<sup>[61]</sup> Moreover, the data confirmed that the UV-vis spectroscopy and TEM results obtained for samples prepared at  $r > 10^9:1$  (see Fig. 2a, curve iv and Fig. 2e, respectively) were correlated and associated with the presence of large compact isotropic aggregates.

Simulations of 1D superstructures based on the linear assembly of increasing numbers of 13 nm diameter Au nanoparticles into non-branched, non-looped linear chains produced spectra that qualitatively reproduced the experimental results and hence supported the TEM observations that the Au nanoparticle chains extend in length with time or increased concentrations of MEA. In agreement with previous results,<sup>[62]</sup> the simulated spectra showed a progressive decrease in the

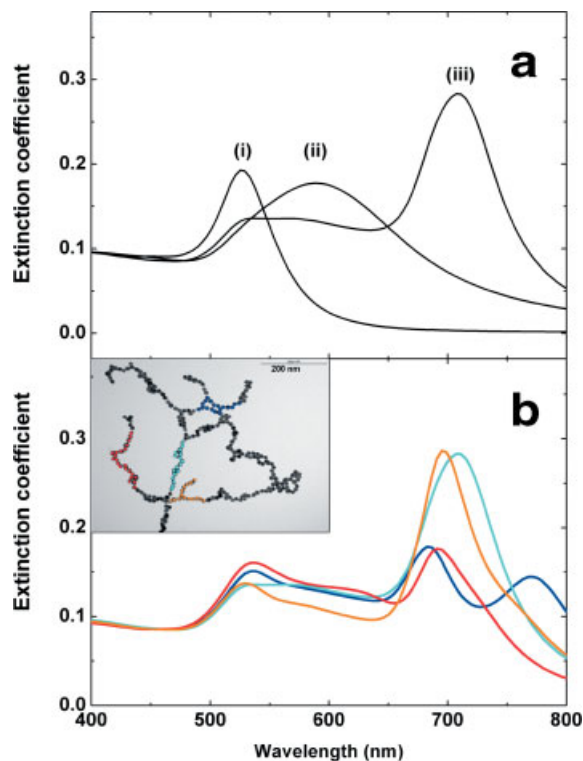


**Figure 4.** a) Simulated spectra of i) isolated Au nanoparticles, ii) compact isotropic Au aggregate containing 245 Au nanoparticles, and iii) distorted non-branched Au nanoparticles chain containing 17 Au nanoparticles. b) Simulated spectra for various chain defects (loops (navy blue), "zig-zags" (red), and Y-junctions (orange)) and superimposed simulated spectrum for a realistic chain (cyan). Corresponding topological arrangement of defects are shown color-coded in the experimental TEM image (inset).

intensity of the 520 nm peak as well as the appearance of a longitudinal plasmon band of increasing intensity which shifted to lower energy with larger numbers of nanoparticles due to enhanced longitudinal coupling. However, compared with the experimental spectra, the simulated longitudinal band was narrower, and red-shifted only to 650 nm compared with an experimental value of 705 nm. A higher level of refinement was achieved by incorporating topological distortions in the chains in place of a strictly linear assembled superstructure. The resulting calculated spectra of realistic chains showed a minor 520 nm transverse band and a dominant longitudinal band at 700 nm (Fig. 4a, curve iii), and reproduced all the main features of the experimental data obtained from networks formed, for example, at  $r = 3000:1$ . Nevertheless, distortions in chain topography were not sufficient to accurately simulate the observed broadness or asymmetry of the experimental longitudinal band, as shown for example in Figures 2a (curve iii) and 3a (curve vi). These features were, however, effectively simulated by incorporation of loops, zigzags, and bifurcations in theoretical models of the extended branched chain networks. As shown in Figure 4b, experimental maps of such topological features were identified within networks obtained from TEM images (Fig. 4b, inset) and used in the dipole–dipole approximation (DDA) code (see Experimental) to calculate the corresponding spectra for these components. Taken together, superimposition of these deviations gave a broader longitudinal plasmon resonance centered at 700 nm compared with a simple distorted chain structure. Interestingly, the spectra associated with Y-junction and zigzag defects revealed single broad peaks at slightly higher energies than 700 nm, whilst the spectrum arising from the loop domains showed the presence of two bands around 680 and 770 nm. In each case, the transverse plasmon at 520 nm remained virtually unchanged.

The results demonstrate that accurate representations of the optical spectra of self-assembled 1D metallic nanoparticle arrays can be computed by use of the DDA method. Various topographical defects such as chain-length polydispersity, nonlinearity, branching points, and looping can be modeled and integrated to account for the statistical broadening of the longitudinal plasmon band. Significantly, accurate simulation of the energy of the longitudinal peak required a refractive index ( $n$ ) for the surrounding media of 1.6–1.7, which is higher than that of pure water. This was consistent, however, with the presence of surface-adsorbed MEA and citrate ligands, which have  $n$  values of ca. 1.5.

The above investigations demonstrate an unusual self-assembly process in which highly anisotropic 1D arrays of isometric Au nanoparticles are spontaneously assembled in the absence of extraneous templates. Onset of chain assembly occurs relatively abruptly at  $r \geq 1500:1$ , suggesting that significant levels of ligand exchange of citrate ions by MEA are required to produce an attractive electric dipole moment capable of overcoming the interparticle electrostatic repulsion forces. We estimate that the monolayer coverage of each nanoparticle with a mean surface area of 530 nm<sup>2</sup> (diameter

$d = 13$  nm) corresponds to approximately 2600 MEA molecules, assuming an average coverage of 0.33 MEA molecules per Au surface atom.<sup>[63]</sup> Consequently, chain formation is triggered at a molar ratio below that needed for complete MEA capping of each nanoparticle, suggesting that the presence of a mixed citrate/MEA stabilization shell is responsible for the generation of a permanent electric dipole moment on each particle. Indeed, Stellacci and co-workers showed that mixed self-assembled monolayers on metal nanoparticles spontaneously undergo microphase separation into domains.<sup>[59]</sup> In our case, spatial partitioning of the neutral MEA and charged citrate capping ligands could be driven by intermolecular interaction between neighboring MEA hydroxyalkyl chains and/or specific interactions of MEA head groups with a subset of exposed crystallographic faces of the twinned Au nanoparticles.<sup>[58]</sup> Our results suggest that such a segregation leads to an anisotropic distribution of the residual surface charge and that this extrinsic electric dipole formation is a prerequisite for the uniaxial organization of the isometric Au nanoparticles into short chains at  $r = 1500:1$ .<sup>[54,56]</sup> Further exchange of citrate ions at higher MEA concentrations increases the extent of chain propagation, and beyond a critical chain length the dipolar interaction energy is decreased by introducing junctions that create an extra entropy contribution.<sup>[49,64]</sup> Branched interconnected networks of spherical nanoparticle chains will thus emerge naturally by anisotropic dipolar interactions as reported previously for magnetic nanoparticles or amphiphilic molecules.<sup>[49,65]</sup> Furthermore, interparticle cohesion within the chains and networks could be reinforced by hydrogen bonding between exposed hydroxyl moieties of the surface-adsorbed MEA molecules,<sup>[56]</sup> as well as between unbound thiol end groups in the boundary layers that act as interchain crosslinkers, for example by disulfide bond formation. This situation is observed in the later stages of chain growth, for example at  $r = 5000:1$ , when no isolated nanoparticles could be observed by TEM, and the chains were resistant to limited periods of sonication and exposure to temperatures above 50 °C. Interestingly, extended chain networks are produced at  $r$  values of 10 000:1, which corresponds to an approximately fourfold excess of MEA molecules required for theoretical monolayer coverage, suggesting that competing equilibria between bound and unbound MEA and citrate ligands extends the range of conditions under which highly anisotropic superstructures can emerge. Indeed, isotropic bulk aggregation did not occur extensively until the  $r$  value exceeded 10<sup>9</sup>:1, at which all the citrate ions were presumably displaced and the electric dipole moment reduced to zero.

In conclusion, we have shown that short chains and complex networks of interconnected chains composed of Au nanoparticles can be readily produced by controlled ligand exchange of surface-adsorbed citrate ions with neutral MEA molecules. Experimental optical spectroscopy and computer simulations show that surface plasmons from individual non-contacting nanoparticles are strongly coupled in the resulting 1D metallic superstructures. The self-assembled architectures exhibit remarkable thermal stability in water, and can be easily trans-

ferred to various solid surfaces, thus providing a unique way to fabricate complex sub-wavelength optical waveguides able to transport electromagnetic energy below the diffraction limit.<sup>[5,6,66,67]</sup> We are currently pursuing efforts to demonstrate such nanophotonic devices.

### Experimental

Isometric Au nanoparticles, often in the form of {111} penta-tetrahedrally twinned nanocrystals, were freshly prepared by the standard citrate reduction method [60] and diluted in milli-Q water to reach a concentration of about  $1.9 \times 10^{14}$  particles  $L^{-1}$  (i.e.,  $3.1 \times 10^{-10}$  M). The average size of the nanoparticles was  $13 \pm 2$  nm. The colloidal gold solution was mixed at room temperature with a 14.3 mM aqueous solution of MEA, such that the MEA:Au nanoparticle molar ratio,  $r$ , was varied between  $r = 1:2$  and  $r = 5 \times 10^{10}:1$  by adjusting the added volume of MEA solution. Aliquots were taken at regular intervals and air-dried on carbon-coated copper grids for electron microscopy analysis (JEOL 1200 EX, JEM 2010 TEM). Optical spectra were recorded on Au nanoparticle dispersions using a PerkinElmer Lambda 25 UV-vis spectrometer.

Experimental optical spectra associated with the presence of discrete Au nanoparticles, extended nanoparticle chains, or condensed isotropic aggregates were successfully simulated by calculations based on the self-consistent solution of the electrodynamic response of individual nanoparticles subjected to a combination of incident and scattered fields generated by neighboring metallic particles [62]. The dipole-dipole approximation (DDA) method was applied by modeling each gold nanoparticle as a 13 nm diameter sphere bearing a single dipole and spaced from adjacent particles by 1.0 nm, in accordance with the TEM data. Gold dielectric functions were taken from the literature [68]. Simulations of the extinction spectra associated with chain-like superstructures were initially based on modeling non-branched, non-looped linear arrays with increasing numbers of nanoparticles while maintaining the polarization of the incident electric field parallel to the chain axis [3]. Extinction spectra of complex branched networks of arbitrary shape were investigated by introducing in our DDA code the actual nanoparticles positions extracted from TEM images of several samples.

Received: April 22, 2005

Final version: July 28, 2005

Published online: September 15, 2005

- [1] R. Quidant, J. C. Weeber, A. Dereux, D. Peyrade, C. Girard, Y. Chen, *Phys. Rev. E: Stat., Nonlinear, Soft Matter Phys.* **2002**, *65*, 036616.
- [2] W. L. Barnes, A. Dereux, T. W. Ebbesen, *Nature* **2003**, *424*, 824.
- [3] C. Girard, *Rep. Prog. Phys.* **2005**, *68*, 1883.
- [4] S. A. Maier, P. G. Kik, H. A. Atwater, *Phys. Rev. B: Condens. Matter Mater. Phys.* **2003**, *67*, 205402.
- [5] S. A. Maier, P. G. Kik, H. A. Atwater, S. Meltzer, E. Harel, B. E. Koel, A. A. G. Requicha, *Nat. Mater.* **2003**, *2*, 229.
- [6] W. H. Weber, G. W. Ford, *Phys. Rev. B: Condens. Matter Mater. Phys.* **2004**, *70*, 125429.
- [7] S. I. Bozhevolnyi, J. Erland, K. Leosson, P. M. W. Skovgaard, J. M. Hvam, *Phys. Rev. Lett.* **2001**, *86*, 3008.
- [8] C. J. Kiely, J. Fink, J. G. Zheng, M. Brust, D. Bethell, D. J. Schiffrin, *Adv. Mater.* **2000**, *12*, 640.
- [9] A. G. Nassiopoulou, A. Zoy, V. Ioannou-Sougleridis, A. Olzierski, A. Travlos, J. L. Martinez-Albertos, B. Moore, *Nanotechnology* **2004**, *15*, 352.
- [10] S. R. Hall, W. Shenton, H. Engelhardt, S. Mann, *ChemPhysChem* **2001**, *2*, 184.
- [11] S. Fullam, H. Rensmo, S. N. Rao, D. Fitzmaurice, *Chem. Mater.* **2002**, *14*, 3643.
- [12] C. A. Mirkin, *Inorg. Chem.* **2000**, *39*, 2258.
- [13] W. Shenton, S. A. Davis, S. Mann, *Adv. Mater.* **1999**, *11*, 449.
- [14] S. Connolly, D. Fitzmaurice, *Adv. Mater.* **1999**, *11*, 1202.
- [15] B. Nikoobakht, Z. L. Wang, M. A. El-Sayed, *J. Phys. Chem. B* **2000**, *104*, 8635.
- [16] E. Dujardin, L. B. Hsin, C. R. C. Wang, S. Mann, *Chem. Commun.* **2001**, 1264.
- [17] K. K. Caswell, J. N. Wilson, U. H. F. Bunz, C. J. Murphy, *J. Am. Chem. Soc.* **2003**, *125*, 13914.
- [18] K. G. Thomas, S. Barazzouk, B. I. Ipe, S. T. S. Joseph, P. V. Kamat, *J. Phys. Chem. B* **2004**, *108*, 13066.
- [19] M. Li, H. Schnablegger, S. Mann, *Nature* **1999**, *402*, 393.
- [20] Z. Y. Tang, N. A. Kotov, *Adv. Mater.* **2005**, *17*, 951.
- [21] J. J. Penninkhof, A. Polman, L. A. Sweatlock, S. A. Maier, H. A. Atwater, A. M. Vredenberg, B. J. Kooi, *Appl. Phys. Lett.* **2003**, *83*, 4137.
- [22] L. Nagle, D. Ryan, S. Cobbe, D. Fitzmaurice, *Nano Lett.* **2003**, *3*, 51.
- [23] S. L. Burkett, S. Mann, *Chem. Commun.* **1996**, 321.
- [24] D. B. Zhang, L. M. Qi, J. M. Ma, H. M. Cheng, *Chem. Mater.* **2001**, *13*, 2753.
- [25] S. Minko, A. Kiriy, G. Gorodyska, M. Stamm, *J. Am. Chem. Soc.* **2002**, *124*, 10192.
- [26] A. H. Bae, M. Numata, T. Hasegawa, C. Li, K. Kaneko, K. Sakurai, S. Shinkai, *Angew. Chem Int. Ed.* **2005**, *44*, 2030.
- [27] E. Braun, Y. Eichen, U. Sivan, G. Ben-Yoseph, *Nature* **1998**, *391*, 775.
- [28] K. Keren, M. Krueger, R. Gilad, G. Ben-Yoseph, U. Sivan, E. Braun, *Science* **2002**, *297*, 72.
- [29] A. Kumar, M. Pattarkine, M. Bhadbhade, A. B. Mandale, K. N. Ganesh, S. S. Datar, C. V. Dharmadhikari, M. Sastry, *Adv. Mater.* **2001**, *13*, 341.
- [30] M. Mertig, L. C. Ciacchi, R. Seidel, W. Pompe, A. De Vita, *Nano Lett.* **2002**, *2*, 841.
- [31] O. Harnack, W. E. Ford, A. Yasuda, J. M. Wessels, *Nano Lett.* **2002**, *2*, 919.
- [32] F. Patolsky, Y. Weizmann, O. Lioubashevski, I. Willner, *Angew. Chem. Int. Ed.* **2002**, *41*, 2323.
- [33] M. G. Warner, J. E. Hutchison, *Nat. Mater.* **2003**, *2*, 272.
- [34] R. Djalali, Y. Chen, H. Matsui, *J. Am. Chem. Soc.* **2002**, *124*, 13660.
- [35] X. Y. Fu, Y. Wang, L. X. Huang, Y. L. Sha, L. L. Gui, L. H. Lai, Y. Q. Tang, *Adv. Mater.* **2003**, *15*, 902.
- [36] T. Scheibel, R. Parthasarathy, G. Sawicki, X. M. Lin, H. Jaeger, S. L. Lindquist, *Proc. Natl. Acad. Sci. USA* **2003**, *100*, 4527.
- [37] M. Reches, E. Gazit, *Science* **2003**, *300*, 625.
- [38] I. A. Banerjee, L. T. Yu, R. I. MacCuspie, H. Matsui, *Nano Lett.* **2004**, *4*, 2437.
- [39] S. Behrens, K. Rahn, W. Habicht, K. J. Bohm, H. Rosner, E. Dinjus, E. Unger, *Adv. Mater.* **2002**, *14*, 1621.
- [40] E. Dujardin, C. Peet, G. Stubbs, J. N. Culver, S. Mann, *Nano Lett.* **2003**, *3*, 413.
- [41] M. Knez, M. Sumser, A. M. Bittner, C. Wege, H. Jeske, T. P. Martin, K. Kern, *Adv. Funct. Mater.* **2004**, *14*, 116.
- [42] C. B. Mao, C. E. Flynn, A. Hayhurst, R. Sweeney, J. F. Qi, G. Georgiou, B. Iverson, A. M. Belcher, *Proc. Natl. Acad. Sci. USA* **2003**, *100*, 6946.
- [43] T. W. Ebbesen, H. Hiura, M. E. Bisher, M. M. J. Treacy, J. L. Shreeve-Keyer, R. C. Haushalter, *Adv. Mater.* **1996**, *8*, 155.
- [44] D. Ugarte, A. Châtelain, W. A. de Heer, *Science* **1996**, *274*, 1897.
- [45] L. M. Ang, T. S. A. Hor, G. Q. Xu, C. H. Tung, S. P. Zhao, J. L. S. Wang, *Chem. Mater.* **1999**, *11*, 2115.
- [46] S. Fullam, D. Cottell, H. Rensmo, D. Fitzmaurice, *Adv. Mater.* **2000**, *12*, 1430.
- [47] B. Xue, P. Chen, Q. Hong, J. Y. Lin, K. L. Tan, *J. Mater. Chem.* **2001**, *11*, 2378.
- [48] M. J. Moughaddam, S. Taylor, M. Gao, S. M. Huang, L. M. Dai, M. J. McCall, *Nano Lett.* **2004**, *4*, 89.

- [49] T. Tlusty, S. A. Safran, *Science* **2000**, *290*, 1328.  
 [50] Z. Y. Tang, N. A. Kotov, M. Giersig, *Science* **2002**, *297*, 237.  
 [51] Z. Y. Tang, B. Ozturk, Y. Wang, N. A. Kotov, *J. Phys. Chem. B* **2004**, *108*, 6927.  
 [52] J. Li, X. Hong, D. Li, K. Zhao, L. Wang, H. Z. Wang, Z. L. Du, J. H. Li, Y. B. Bai, T. J. Li, *Chem. Commun.* **2004**, 1740.  
 [53] B. V. Enüstün, J. Turkevich, *J. Am. Chem. Soc.* **1963**, *85*, 3317.  
 [54] J. H. Liao, Y. Zhang, W. Yu, L. N. Xu, C. W. Ge, J. H. Liu, N. Gu, *Colloids Surf., A* **2003**, *223*, 177.  
 [55] J. Y. Chang, J. J. Chang, B. Lo, S. H. Tzing, Y. C. Ling, *Chem. Phys. Lett.* **2003**, *379*, 261.  
 [56] A. N. Shipway, M. Lahav, R. Gabai, I. Willner, *Langmuir* **2000**, *16*, 8789.  
 [57] B. Nikoobakht, M. A. El-Sayed, *Langmuir* **2001**, *17*, 6368.  
 [58] C. J. Johnson, E. Dujardin, S. A. Davis, C. J. Murphy, S. Mann, *J. Mater. Chem.* **2002**, *12*, 1765.  
 [59] A. M. Jackson, J. W. Myerson, F. Stellacci, *Nat. Mater.* **2004**, *3*, 330.  
 [60] J. J. Storhoff, R. Elghanian, R. C. Mucic, C. A. Mirkin, R. L. Letsinger, *J. Am. Chem. Soc.* **1998**, *120*, 1959.  
 [61] J. J. Storhoff, A. A. Lazarides, R. C. Mucic, C. A. Mirkin, R. L. Letsinger, G. C. Schatz, *J. Am. Chem. Soc.* **2000**, *122*, 4640.  
 [62] A. A. Lazarides, G. C. Schatz, *J. Phys. Chem. B* **2000**, *104*, 460.  
 [63] M. Hyun, C. K. Rhee, *Bull. Korean Chem. Soc.* **2001**, *22*, 213.  
 [64] A. Zilman, T. Tlusty, S. A. Safran, *J. Phys.: Condens. Matter* **2003**, *15*, S57.  
 [65] T. Tlusty, S. A. Safran, *Philos. Trans. R. Soc. London, Ser. A* **2001**, *359*, 879.  
 [66] D. S. Citrin, *Nano Lett.* **2004**, *4*, 1561.  
 [67] Q. H. Wei, K. H. Su, S. Durant, X. Zhang, *Nano Lett.* **2004**, *4*, 1067.  
 [68] E. D. Palik, *Handbook of Optical Constants of Solids*, Academic, San Diego, CA **1998**.

## Multiscale Nanopatterns Templated from Two-Dimensional Assemblies of Photoresist Particles\*\*

By Jun Hyuk Moon, Se Gyu Jang, Jong-Min Lim, and Seung-Man Yang\*

Photolithography has been used to fabricate multiscale patterns, which are commonly required for various integrated microdevices. While photolithography precisely transfers multiscale patterns, the feature size of these patterns is restricted

by diffraction-limited resolution scales. Consequently, shorter-wavelength light, such as deep ultraviolet (DUV) or extreme ultraviolet (EUV), must be used to reduce the minimum feature size to the submicrometer scale. However, this still requires expensive lithography devices.<sup>[1]</sup> As an alternative route, template-induced lithography using self-organized colloidal particles,<sup>[2]</sup> block copolymers,<sup>[3]</sup> emulsions,<sup>[4]</sup> and self-assembled monolayered molecules<sup>[5]</sup> has been developed for simple and cheap nanometer-scale pattern formation.

Colloidal lithography (CL) uses self-assembled arrays of colloidal particles as sacrificial masks, and various functional materials are deposited through the interstitial pores between the particles. For example, the deposition of metals (Co, Ge, Au, Ni, and Ag) or dielectrics (titania, silica, and silicon), in the form of hierarchically patterned arrays, has been demonstrated for various applications, including surface plasmon resonance sensors, catalysts or catalytic supports, photonic crystals, and information-storage devices.<sup>[2b,6]</sup> To date, CL has been used to produce arrays of nanometer-scale “unit atoms”; the size and shape have been manipulated by annealing the colloidal particles,<sup>[6a,6b]</sup> by angle-resolved deposition,<sup>[7]</sup> and by multiple layering of particles.<sup>[8]</sup> However, CL has been applied only for creating periodic patterns on a single-feature scale, mainly with *p6mm* symmetry resulting from two-dimensional (2D) close-packing of colloidal particles. Therefore, it is still necessary to develop a practical CL for fabricating multiscale nanopattern-based devices such as combinatorial catalytic supports,<sup>[9]</sup> photonic crystal waveguides,<sup>[10]</sup> and interferometric biosensors embedded in microfluidic chips.<sup>[11]</sup>

For multiscale patterning by CL, a facile strategy is needed either to arrange colloidal particles in spatially designed patterns or to use colloidal particles of several different sizes. However, it is practically impossible to achieve hierarchical self-organization of polydisperse particles in regular patterns. Meanwhile, self-assembly in a pre-patterned substrate, or field-assisted assembly can be applied for selective deposition of colloidal-particle arrays.<sup>[12]</sup> Recently, a more direct method has been successfully demonstrated by Jiang et al. using a self-assembled template of spherical colloids, which contains photocrosslinkable monomers at the interstices, and a subsequent photolithographic process.<sup>[13]</sup> This approach is practically advantageous in that it is not only compatible with conventional semiconductor-fabrication processes, but it is also able to transfer well-defined complex patterns. Here, we report an alternative photolithography-assisted CL with photocrosslinkable colloidal particles (hereafter, referred to as ‘photoresist particles’).<sup>[14]</sup> In the present method, the colloidal solution was used as prepared, without exchanging the solvent medium with a photopolymerizable monomer solution. The overall strategy is depicted in Scheme 1. First, the photoresist particles with a photoinitiator were deposited and self-organized into a 2D array on a silicon substrate. Following this, in the photolithographic process (UV exposure and post-exposure baking) carried out with designed masks, localized domains of the photoresist-particle array were crosslinked selectively on a micrometer scale. At the same time, the photo-

[\*] Prof. S.-M. Yang, Dr. J. H. Moon,<sup>[†]</sup> S. G. Jang, J.-M. Lim  
 Department of Chemical and Biomolecular Engineering  
 Korea Advanced Institute of Science and Technology  
 373-1 Guseong-dong, Yuseong-gu, Daejeon, 305-701 (Korea)  
 E-mail: smyang@kaist.ac.kr

[†] Present address: Department of Materials Science and Engineering,  
 University of Pennsylvania, Philadelphia, PA 19104, USA.

[\*\*] This work was supported by the National R&D Project for Nano Science and Technology of the Ministry of Commerce, Industry and Energy. Partial support was received from the Center for Nanoscale Mechatronics and Manufacturing through the 21st Century Frontier Research Program (M102 KN010002-05 K1401-00214). The BK21 and CUPS-ERC programs are also acknowledged. We thank Dr. Won Sun Kim and Dr. Jong-Wook Ha for useful discussions.